Form birefringence metal and its plasmonic anisotropy

Liang Feng,[a] Zhaowei Liu,[a] Vitaliy Lomakin, and Yeshaiahu Fainman[a]
Department of Electrical and Computer Engineering, University of California, San Diego, La Jolla, California 92093, USA

(Received 5 November 2009; accepted 4 January 2010; published online 29 January 2010)

We constructed a uniaxial "form birefringence" metal that exhibits different dielectric polarizabilities along different optical axes as well as its supported optical anisotropy of surface plasmon polariton waves. The generated plasmonic index ellipsoid that exists in reciprocal space has been directly mapped and characterized in our experiment. The discovery of this anisotropic plasmonic metamaterial further completes analogy between artificial plasmonic metamaterials and conventional optical crystals, thereby providing opportunities to miniaturize myriad existing optical devices on-a-chip with plasmonics into nanometers scale. © *2010 American Institute of Physics*. [doi:10.1063/1.3299002]

Optical anisotropy originates from atomic scale dipole moments that vary in space depending on the crystal lattice structure. Consequently, such crystals possess indices of refraction that depend on the crystallographic lattice structure and in most general case are described in reciprocal space by an index ellipsoid in three dimensions.[1,2] More recently, space-variant polarizability of isotropic dielectrics has been achieved by creating a deeply subwavelength structure composed of two or more materials such that in electrostatic field approximation it acts similarly to that of an anisotropic crystal, where the subwavelength scale geometry can have average polarizability varying in three dimensions of the medium.[3] These structures called "form birefringence" have also been used for various applications to manipulate the polarization state of the fields in forms that are not possible with natural birefringent crystalline dielectrics.[4–6] Similarly "artificial dielectrics," the electric metamaterial consisting of metallic wires in a host dielectric medium has been proposed and analyzed in both microwave and optical frequencies.[7–11] In the long wavelength approximation regime using the effective medium theory,[12] this reported metal-dielectric composite acts as a slab with hyperbolic dispersion properties that have been used to manipulate the propagating optical fields, showing negative refraction.[13,14]

Recently, plasmonics that uses interaction of light and surface electrons on a metal-dielectric boundary has attracted attention due to its ability to strongly confine light near the interface and intrinsically localize light in small volumes. The utilization of surface plasmon polariton (SPP) can help to create optical field localization devices, enable great functionalities on a nanometer scale and are making an impact due to the extreme field confinement on uniquely suitable applications.[15–19] Note, that although the above reported applications rely on isotropic plasmonic properties of metals, some applications[20] would only be possible by using plasmonic anisotropy. However, since optical properties of natural metals are always isotropic, in practice, it is difficult to realize optical plasmonic anisotropy. In this letter, we propose and experimentally demonstrate for a metal-dielectric composite metamaterial, in contrast to Refs. 13 and 14, composed of dielectrics in a host metal that acts as an anisotropic uniaxial birefringent metal, supporting propagating SPP waves. Our metal-dielectric composite transfers its material birefringence to the SPP's. We construct the effective index ellipsoid of such a metal-dielectric composite and show numerically and experimentally the corresponding SPP modes using the reciprocal space representations.

The form birefringent metal acting as an anisotropic plasmonic metamaterial, schematically depicted in Fig. 1(a), is a two-dimensional array of air nanoholes in a thin metal film implementing a deeply subwavelength periodic structure with periods differing in x and y directions. The effective dielectric constant tensor of this metamaterial can be described as

$$\varepsilon_{\text{eff}} = \begin{pmatrix} \varepsilon_x & 0 & 0 \\ 0 & \varepsilon_y & 0 \\ 0 & 0 & \varepsilon_z \end{pmatrix}, \tag{1}$$

and using the effective medium theory the three diagonal elements are approximately expressed by[12]

$$\varepsilon_x = \varepsilon_m\left(1 - \frac{\pi r^2}{2d_y r}\right) + \varepsilon_0 \frac{\pi r^2}{2d_y r},$$

$$\varepsilon_y = \varepsilon_m\left(1 - \frac{\pi r^2}{2d_x r}\right) + \varepsilon_0 \frac{\pi r^2}{2d_x r},$$

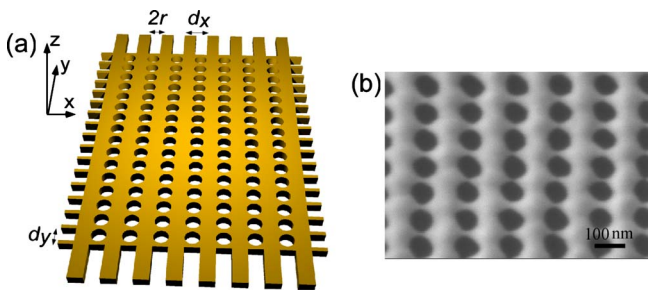

FIG. 1. (Color online) Form birefringence metal acts as an anisotropic plasmonic metamaterial. (a) Schematic of a 55 nm thick Au anisotropic plasmonic metamaterial with the design parameters: d_x=140 nm, d_y=93 nm, and r=35 nm. (b) SEM micrograph of the fabricated structure using FIB milling.

[a]Electronic addresses: lifeng@ucsd.edu, zhaowei@ece.ucsd.edu, and fainman@ece.ucsd.edu.

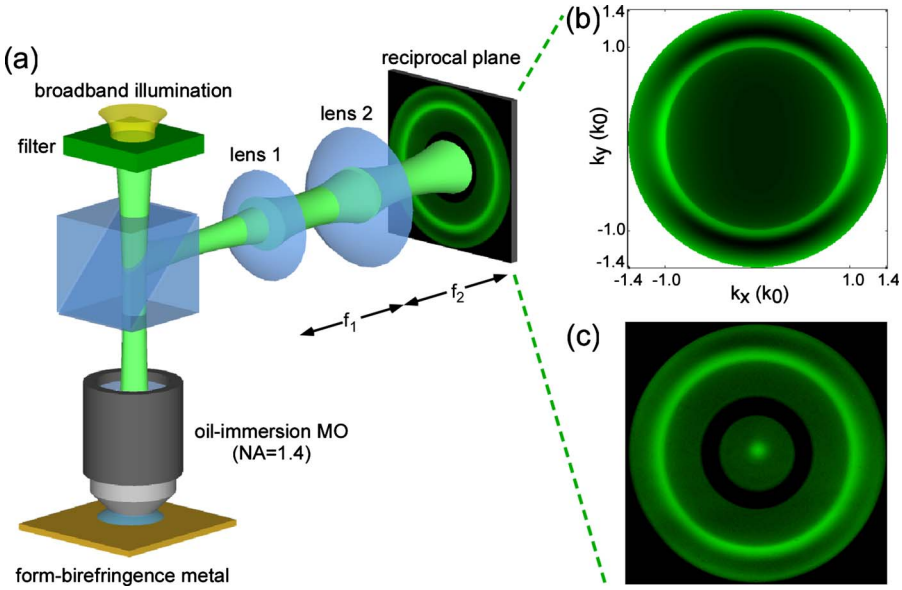

FIG. 2. (Color online) Characterization of SPP's index ellipsoid at the center wavelength of 540 nm. (a) Measurement setup to directly image SPP's index ellipsoid in reciprocal space in the far field, consists of a broadband source, an oil immersion microscope objective with NA=1.4, two lenses, and a CCD camera. (b) Simulated SPP's index ellipsoid in a representation of reflected power distribution in reciprocal space. (c) Experimental imaging of reflection from the metamaterial in reciprocal space. The dark elliptical rings indicate the excitation of anisotropic SPP waves and are the corresponding SPP index ellipsoids.

$$\varepsilon_z = \varepsilon_m\left(1 - \frac{\pi r^2}{d_x d_y}\right) + \varepsilon_0 \frac{\pi r^2}{d_x d_y}, \tag{2}$$

where ε_m and ε_0 are the dielectric constants of metal (e.g., Au) (Ref. 21) and dielectric medium in the nanoholes (e.g., air), respectively, r is the radius of nanoholes, and d_x and d_y are the periods of the deeply subwavelength structure in the x and y directions, respectively. Since all three parameters in Eq. (2) are negative, the constructed metamaterial can be considered as an anisotropic metal. Therefore, it is evident that the different effective dielectric constants will inevitably result in different SPP eigenmodes with their corresponding dispersion relations along the x and the y axes, thus creating optical anisotropy for SPP fields.

To validate our proposed anisotropic plasmonic metal-dielectric metamaterial, we use focused-ion-beam milling to fabricate fine deeply subwavelength features shown in Fig. 1(a) using an Au film (Au was chosen since it is unlikely to be oxidized) on a glass substrate. The scanning electron microscopy (SEM) micrograph of the fabricated structure is shown in Fig. 1(b). The excited SPP modes in the fabricated metamaterial are characterized in reciprocal space by analyzing reflection images [see Fig. 2(a)] obtained from the glass substrate side of the samples inserted in an oil immersion microscope objective (MO) with high numerical aperture (NA=1.4).

Figure 2 shows the numerically simulated and experimentally measured index ellipsoids of SPPs on the artificial form birefringent metal in reciprocal space at the wavelength around 540 nm. A converging unpolarized spherical wave is used as an illumination function to code a wide-band angular momentum of the illumination function to a constant radial position within the illumination circle. Lens 1 and the microscope objective are used to construct a typical 4-f imaging system. The charge coupled device (CCD) camera is located at the focal plane of lens 2 so that it can directly capture the corresponding Fourier transform, which represents the SPP's index ellipsoid in the k space. Some of these spatial frequencies satisfy the phase matching condition and thus excite SPPs. The size of the obtained image is limited by the NA of our MO that corresponds to a free space wavevector of $1.4k_0$. Note that the central dark ring in Fig. 2(c) (i.e., image of the phase ring inside the phase contrast MO) obscures some information but the information of interest here occurs at larger wavevectors. The bright circle represents the boundary of the illumination at the angle corresponding to total internal reflection (TIR) when the transverse component of the illumination wavevector is k_0. Outside this TIR circle, an elliptical dark ring caused by excitation of SPPs manifests the optical plasmonic anisotropy of the excited SPP waves. From this index ellipsoid, we can also retrieve experimentally the effective wavevectors of SPP modes propagating along x and y optical axes as well as other azimuthal angles.

With considering the boundary continuity, the eigenvectors of SPPs along x and y axes yield

$$k_{spp}^{x,y} = k_0 \sqrt{\frac{\varepsilon_0 \varepsilon_z (\varepsilon_{x,y} - \varepsilon_0)}{\varepsilon_{x,y}\varepsilon_z - \varepsilon_0 \varepsilon_0}}, \tag{3}$$

where k_0 represents the wavevector of light in free space. The experimentally measured wavevectors from Fig. 2 are integrated into Fig. 3 for comparison with the analytical calculations using Eq. (3) and numerical simulations in which the wavevectors of SPPs is determined as the positions of dips in the simulated reflection spectra. The index ellipsoid

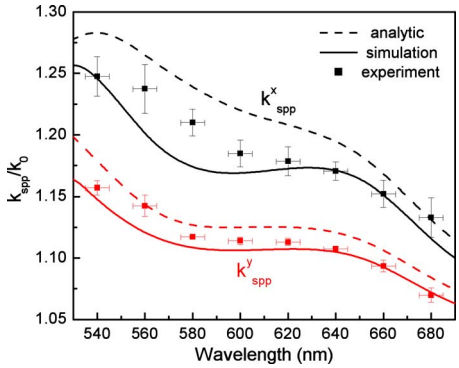

FIG. 3. (Color online) Anisotropic SPP dispersion relations. Upper and lower symbols represent SPP's wavevectors along the x and y directions, respectively. Solid curve, dashed curve, and square dot correspond to the data retrieved from analytical calculations according to Eqs. (1)–(3), numerical simulations and experimental measurements, respectively. For experimental data, the error-bar in wavelengths indicates the bandwidth (10 nm) of the bandpass filters used in the experimental measurement.

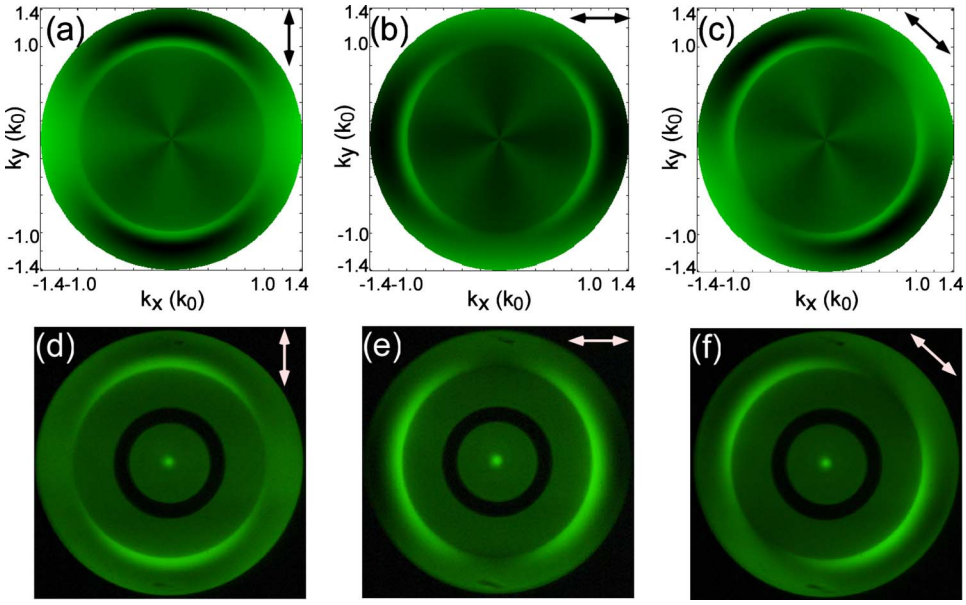

FIG. 4. (Color online) Simulated and measured SPP index ellipsoids with different polarization orientations. [(a)–(c)] Simulated reflection map in reciprocal space. [(d)–(f)] Experimental imaging of reflection in reciprocal space. The polarization states in [(a), (d)], [(b), (e)], and [(c), (f)] are oriented along the *y*, *x*, and at 45°-axis, respectively.

and SPP's dispersion relations of wavevectors are measured as a function of optical wavelength by analyzing images obtained using a series of 10 nm bandpass interference filters in the spectral range of interest, i.e., from 540 to 680 nm. The plasmonic anisotropy in the range of interest attributes to the effective dipole moments engineered in an "artificial-atomic" scale with deep subwavelength features that vary in space depending on the crystal lattice of our form birefringent metal. The effective SPP indices in different directions vary since the plasmonic field interactions between unit cells strongly change with different duty cycles and dipole orientations, and thus manifest different averaged plasmonic E-fields in both individual unit cells and holes.

Polarized illumination was used to extract more detailed features and properties of the excited SPP modes on our form birefringent metal. Depending on the state of polarization of the illuminating field, only a fraction of SPP modes on the index ellipsoid will be excited. Both measured and simulated results are consistent with the results shown in Fig. 2 obtained with unpolarized illumination. When the polarization of the illumination field is along one of the optic axes [see Figs. 4(a), 4(b), 4(d), and 4(e)], a symmetric SPP modes distribution with respect to the direction of the polarization is observed. Note, that the SPP wavevector propagating along the *x* direction has a relatively larger wavevector but a smaller Quality factor with a wider spatial frequency bandwidth. When the illumination field is polarized at 45° with respect to the optic axes, the SPP modes distribution is clearly asymmetric along the *x* and *y* directions, suggesting plasmonic anisotropy. Data on SPP modes wavevectors extracted from Figs. 4(c) and 4(f) are found in good agreement with the results obtained with unpolarized illumination (Fig. 2) and other polarizations in Fig. 4.

Analog to optical birefringent crystals in nature, an artificial form birefringence metal has been constructed and demonstrated different polarizabilities along different optical axes. This material anisotropy leads to optical plasmonic anisotropy of excited SPP modes. It is worth noting that the concept of form birefringence metal is not limited within the specific case shown above. The three-dimensional case can be designed more complicated to adapt more complex Bravais crystal lattices and thus realize a bi- or multiaxial anisotropic metal. Therefore, form-birefringence metals provide more flexibility in engineering inherent metal properties for complex homogeneous and inhomogeneous plasmonic devices that highly demand a wide-range adiabatic change of metal's dielectric constant and SPP's index in optical circuit design.

L.F. thanks Dr. Dong Yan at UC Riverside for his help in FIB fabrication. This work is supported by NSF, DARPA, and NSF CIAN ERC.

[1] A. Yariv and P. Yeh, *Optical Waves in Crystals: Propagation and Control of Laser Radiation* (Wiley, New York, 2003).
[2] M. Born and E. Wolf, *Principles of Optics: Electromagnetic Theory of Propagation, Interference and Diffraction of Light* (Cambridge University Press, Cambridge, 1999).
[3] I. Richter, P. C. Sun, F. Xu, and Y. Fainman, Appl. Opt. **34**, 2421 (1995).
[4] F. Xu, R. C. Tyan, P. C. Sun, Y. Fainman, C. C. Cheng, and A. Scherer, Opt. Lett. **21**, 1513 (1996).
[5] R. C. Tyan, A. A. Salvekar, H. P. Chou, C. C. Cheng, A. Scherer, F. Xu, P. C. Sun, and Y. Fainman, J. Opt. Soc. Am. A Opt. Image Sci. Vis **14**, 1627 (1997).
[6] U. Levy, M. Abashin, K. Ikeda, A. Krishnamoorthy, J. Cunningham, and Y. Fainman, Phys. Rev. Lett. **98**, 243901 (2007).
[7] W. E. Kock, Proc. IRE **34**, 828 (1946).
[8] J. Brown, Proc. Inst. Electr. Eng. **100**, 51 (1953).
[9] W. Rotman, IRE Trans. Antennas Propag. **10**, 82 (1962).
[10] J. B. Pendry, A. J. Holden, W. J. Stewart, and I. Youngs, Phys. Rev. Lett. **76**, 4773 (1996).
[11] D. R. Smith and N. Kroll, Phys. Rev. Lett. **85**, 2933 (2000).
[12] S. M. Rytov, Sov. Phys. JETP **2**, 466 (1956).
[13] J. Yao, Z. Liu, Y. Liu, Y. Wang, C. Sun, G. Bartal, A. Stacy, and X. Zhang, Science **321**, 930 (2008).
[14] J. Elser, R. Wangberg, V. A. Podolskiy, and E. E. Narimanov, Appl. Phys. Lett. **89**, 261102 (2006).
[15] P. Zijlstra, J. W. M. Chon, and M. Gu, Nature **459**, 410 (2009).
[16] L. Cao, J. S. White, J. S. Park, J. A. Schuller, B. M. Clemens, and M. L. Brongersma, Nature Mater. **8**, 643 (2009).
[17] K. F. MacDonald, Z. L. Samson, M. I. Stockman, and N. I. Zheludev, Nat. Photonics **3**, 55 (2009).
[18] R. F. Oulton, V. J. Sorger, T. Zentgraf, R. M. Ma, C. Gladden, L. Dai, G. Bartal, and X. Zhang, Nature (London) **461**, 629 (2009).
[19] S. I. Bozhevolnyi, V. S. Volkov, E. Devaus, J. Y. Laluet, and T. W. Ebbesen, Nature (London) **440**, 508 (2006).
[20] J. Elser and V. A. Podolskiy, Phys. Rev. Lett. **100**, 066402 (2008).
[21] E. D. Palik, *Handbook of Optical Constants of Solids* (Academic, New York, 1985).